AIAA JOURNAL
Vol. 30, No. 12, December 1992

Flutter Suppression of Thin Airfoils Using Active Acoustic Excitations

Pong-Jeu Lu* and Li-Jeng Huang†
National Cheng Kung University, Tainan, Taiwan 70101, Republic of China

A theoretical analysis of the flutter suppression of oscillating thin airfoils using active acoustic excitations in incompressible flow is presented. Closed-form unsteady aerodynamic loads induced by a simple harmonic acoustic excitation on a typical section model are derived. The acoustic wave generator used in the present flutter suppression analysis is activated by a state feedback control law that particularly takes into account the relative phases between the sensed states and the acoustic excitations. The flutter boundaries of the typical section, with and without the acoustic excitations, are evaluated using both the *V-g* and root-locus methods. The results show that, although the acoustic wave is a weak flow perturbation per se, the induced aerodynamic loads can be large enough to be employed as the flutter control forces. The circulatory part that makes the flow satisfy the Kutta condition at the trailing edge contributes the most to the magnitude and phase of the acoustically induced airloads, in particular when the acoustic excitation position is placed close to the trailing edge. Parametric study reveals that both the phase of the feedback gain constant and the acoustic excitation position are critical for the present new flutter suppression technique.

Nomenclature

a = location of the elastic axis
b = semichord length
H_c = nondimensional sound source strength, $\Phi_c/b^2\omega_\alpha$
k = reduced frequency, $\omega b/U$
L = lift per unit span
M_α = pitching moment per unit span, positive nose up
m_s = mass per unit span of the typical section
Q_c = nondimensional monopole strength, Φ_c/bU
r_c,θ_c = polar coordinates of the sound source in Joukowski transformed domain
r_α = nondimensional radius of gyration
$\bar{s}$ = nondimensional Laplace transform variable, s/ω_α
$\bar{t}$ = nondimensional time, $\omega_\alpha t$
$\bar{U}$ = nondimensional freestream speed, $U/b\omega_\alpha$
x_c,z_c = nondimensional coordinates of sound source
x_α = static unbalance
γ_a,γ_w = vorticity strengths along airfoil and wake, respectively
δ = Dirac delta function
Φ_c = volume flow rate or strength of the sound source
η = air-to-structure mass ratio, $\rho b^2/m_s$
ρ = air density
σ = nondimensional Laplace transform variable, sb/U
τ = nondimensional time, tU/b
ω = circular frequency
$\bar{\omega}$ = nondimensional circular frequency, ω/ω_α
ω_h,ω_α = uncoupled plunging and pitching natural frequencies

Subscripts
F = flutter
op = open loop
s = structural

Superscripts
C = acoustically induced
CC = acoustically induced circulatory part
CNC = acoustically induced noncirculatory part
$\sim$ = nondimensional variables
$\cdot$ = time derivative, d/dt
$\hat{}$ = complex magnitude in the Laplace transform domain
$\tilde{}$ = complex magnitude in the frequency domain

Received Aug. 9, 1991; revision received May 12, 1992; accepted for publication May 26, 1992.

*Associate Professor, Institute of Aeronautics and Astronautics. Member AIAA.
†Graduate Research Assistant, Institute of Aeronautics and Astronautics.

I. Introduction

In the past decades, extensive research has been carried out aimed at developing active flutter suppression and control techniques.[1-4] To actively suppress the flutter, control forces have to be created to counteract the wing flutter motions. The aerodynamic control surfaces driven by the hydraulic power units, which include leading- and trailing-edge flaps, ailerons, spoilers, tailerons, and additional vanes, are often employed for flutter suppression and gust alleviation. Although these active control techniques using aerodynamic control surfaces are promising as compared with the passive methods, there exist new difficulties, such as the design of the feedback control laws and the implementation of the hydroservo systems, that plagued the development of the active flutter suppression technique. A specific problem is the intrinsic characteristic of the servomechanism, namely, the hydraulic actuator is usually sluggish in response and hence cannot cope with the high-frequency oscillations.

Active acoustic excitation techniques have been widely adopted in many fluid dynamics applications nowadays. In the study of noise control, the acoustic equipment is used in conjunction with the active sound control strategy that has been known as *antisound*. Ffowcs Williams[5] has advocated this antisound concept and emphasized that, in principle, unsteady linear secondary fields can artificially be produced in antiphase with the primary fields to result in a suppression of the primary fields. Since many basic aeronautical fluid problems are rooted in the interactions among acoustic wave and other shear or instability waves,[6] it is natural that the manipulation of the acoustic wave may find application in various aerodynamic areas, significantly broadening its usefulness from the original discipline of noise control. Specific aviation applications range from the basic mixing and jet flows,[7] combustion instabilities,[8] and separation flow controls,[9] to the practical engine problems such as surge,[10] rotating stall and buzz,[11] and screech phenomena[12] of the reheating system.

Acoustic devices have the advantage of being simple in hardware, and, most importantly, the operational frequency

range is wide and the response is quick in comparison with conventional aerodynamic control surfaces. It would be interesting to aeroservoelasticians if active sound control could be applied to the flutter suppression or gust alleviation problems. Huang[13] has first successfully conducted a wind-tunnel experiment to show that an appropriately operated loudspeaker system can stabilize a fluttering airfoil and presented a preliminary theory to explain the underlying mechanism. He noticed that the loudspeaker-induced aerodynamic forces are large, and he used a *hydraulic analogy* to explain that the amplification effect comes mainly from the area of the airfoil exposed to the acoustic wave field. As will be shown in the present paper, this hydraulic analogy is not sufficient to explain the mechanism of the acoustic flutter suppression phenomenon. It is the conversion and amplification of the incident acoustic wave into shedding vortices from the trailing edge, known as the *trailing-edge receptivity*,[14-16] that holds the key to the present acoustic flutter suppression technique. The analysis presented in the following sections will be valuable for elucidating the underlying mechanism and for identifying the important parameters involved.

II. Equations of Motion for a Typical Section Model

A bending-torsion typical section model equipped with an internal acoustic control device is shown in Fig. 1. The sound waves, generated by an acoustic generator such as a loudspeaker, are transmitted through a duct and are emitted into the airstream from the slot. The equations of motion for this two-dimensional dynamic system can be written as

$$\boldsymbol{M}_s\ddot{\boldsymbol{q}} + \omega_\alpha^2\boldsymbol{K}_s\boldsymbol{q} = \frac{1}{m_s b^2}\{\boldsymbol{f}^A + \boldsymbol{f}^C\} \tag{1}$$

The vectors $\boldsymbol{f}^A$ and $\boldsymbol{f}^C$ represent the aerodynamic loads (lift and pitching moment) induced by the airfoil motion and the acoustic excitation, respectively, which take the following forms:

$$\boldsymbol{f}^A = [-bL^A, M_\alpha^A]^T, \qquad \boldsymbol{f}^C = [-bL^C, M_\alpha^C]^T$$

The generalized coordinate vector $\boldsymbol{q}$ consists of the plunging h/b and the pitching α modes,

$$\boldsymbol{q} = [h/b, \alpha]^T$$

The structural mass and stiffness matrices $\boldsymbol{M}_s$ and $\boldsymbol{K}_s$ are defined as follows:

$$\boldsymbol{M}_s = \begin{bmatrix} 1 & x_\alpha \\ x_\alpha & r_\alpha^2 \end{bmatrix}, \qquad \boldsymbol{K}_s = \begin{bmatrix} (\omega_h/\omega_\alpha)^2 & 0 \\ 0 & r_\alpha^2 \end{bmatrix}$$

In the present analysis, we assume that the oscillating amplitude of the typical section and the acoustic excitation are both small. Thus the aerodynamic forces can be obtained using linearized potential flow theory. Since we are interested in studying the fundamental mechanism involved in the acoustic flutter suppression phenomenon, two-dimensional incompressible unsteady flow theory is adopted as the aerodynamic tool for the present investigation.

Using the superposition principle, the unsteady aerodynamic loads can be split into two uncoupled parts, one induced by the airfoil motion in the absence of acoustic excitation, and the other induced by an active acoustic excitation with the typical section held fixed and aligned in the freestream direction. Therefore, the velocity potential can be decomposed into

$$\phi(x,z,t) = \phi^A(x,z,t) + \phi^C(x,z,t)$$

in which the superscripts A and C refer to airfoil motion and acoustic excitation, respectively. These two fields are termed, in the spirit of antisound, as primary (ϕ^A) and secondary (ϕ^C) fields in the following discussions.

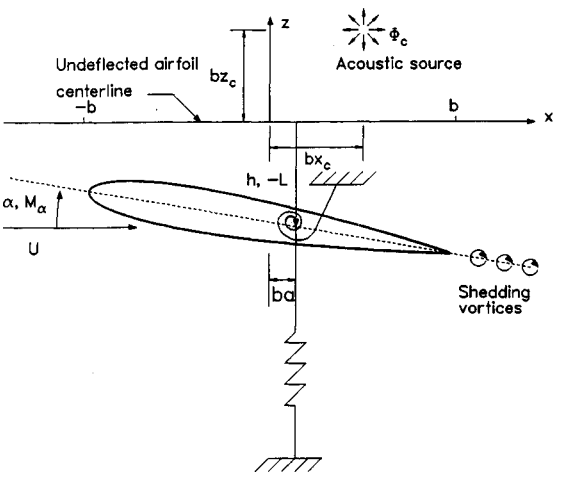

Fig. 1 Model of a typical section with acoustic excitation.

The aerodynamic loads induced by a harmonically oscillating typical section in the two-dimensional incompressible flow have been obtained by Theodorsen[17] and Bisplinghoff et al.[18] and can be written as

$$\tilde{\boldsymbol{f}}^A = \rho U^2 b^2[-k^2\boldsymbol{M}_{anc} + ik\boldsymbol{B}_{anc} + \boldsymbol{K}_{anc} + (ik\boldsymbol{B}_{ac} + \boldsymbol{K}_{ac})C(k)]\tilde{\boldsymbol{q}} \tag{2}$$

where $\boldsymbol{M}_{anc}$, $\boldsymbol{B}_{anc}$, and $\boldsymbol{K}_{anc}$ denote the aerodynamic noncirculatory mass, damping, and stiffness matrices, and $\boldsymbol{B}_{ac}$ and $\boldsymbol{K}_{ac}$ denote the aerodynamic circulatory damping and stiffness matrices, respectively. Their definitions are given as follows:

$$\boldsymbol{M}_{anc} = \begin{bmatrix} -\pi & \pi a \\ \pi a & -\pi(\tfrac{1}{8} + a^2) \end{bmatrix} \quad \boldsymbol{B}_{anc} = \begin{bmatrix} 0 & -\pi \\ 0 & -\pi(\tfrac{1}{2} - a) \end{bmatrix}$$

$$\boldsymbol{K}_{anc} = \begin{bmatrix} 0 & 0 \\ 0 & 0 \end{bmatrix} \quad \boldsymbol{B}_{ac} = \begin{bmatrix} -2\pi & -2\pi(\tfrac{1}{2} - a) \\ 2\pi(\tfrac{1}{2} + a) & 2\pi(\tfrac{1}{2} + a)(\tfrac{1}{2} - a) \end{bmatrix}$$

$$\boldsymbol{K}_{ac} = \begin{bmatrix} 0 & -2\pi \\ 0 & 2\pi(\tfrac{1}{2} + a) \end{bmatrix}$$

where $C(k)$ is the well-known Theodorsen's function.[17,18]

The aerodynamic loads $\tilde{\boldsymbol{f}}^C$ induced on a fixed flat plate due to harmonic acoustic excitations will be derived in the next section.

III. Acoustically Induced Unsteady Aerodynamic Loads

In the present analysis, the acoustic source is modeled as a two-dimensional monopole with time-varying volumetric strength $\Phi_c(t)$. We will first derive solutions for the external excitation model and then obtain the internal excitation solutions from the former by putting the source onto the airfoil surface.

For an incompressible medium, the governing equation for the acoustically induced flowfield can be expressed as

$$\left(\frac{\partial^2}{\partial x^2} + \frac{\partial^2}{\partial z^2}\right)\phi^C(x,z,t) = \Phi_c(t)\delta(x - x_c)\delta(z - z_c) \tag{3}$$

The solution of Eq. (3) should satisfy the vanishing far-field condition and the flow tangency boundary condition on the solid surfaces. In addition, for low-frequency oscillations, the Kutta condition at the sharp trailing edge should be satisfied to result in a smooth flow there.

The solutions of this boundary-value problem can be obtained via conformal mapping and theories of complex variables. Based on the principle of superposition, the present

problem can be split into two elementary parts: the noncirculatory part, for which the flowfield satisfies only the solid tangential boundary condition, and the circulatory part that consists of the shedding vortices and the corresponding images. The strength of this shedding vortex sheet will be determined so as to make the acoustically induced flow satisfy the Kutta condition at the trailing edge. Figure 2 is a schematic illustrating these two parts of the solution in the Joukowski transformed domain. The unsteady airloads induced by a harmonic acoustic monopole with the strength

$$\Phi_c(t) = \tilde{\Phi}_c e^{i\omega t} \tag{4}$$

can be shown the have the forms[19]

$$\Delta\tilde{C}_p^C = -2\left(\frac{ik}{2\pi}\ell_n\left[\frac{1+r_c^2-2r_c\cos(\theta+\theta_c)}{1+r_c^2-2r_c\cos(\theta-\theta_c)}\right]\right.$$

$$+\left\{\frac{-1}{2\pi}\left[\frac{2r_c\sin(\theta+\theta_c)}{1+r_c^2-2r_c\cos(\theta+\theta_c)}\right.\right.$$

$$\left.\left.-\frac{2r_c\sin(\theta-\theta_c)}{1+r_c^2-2r_c\cos(\theta-\theta_c)}\right]\frac{1}{\sin\theta}\right.$$

$$\left.-2E_5\left[\cot\theta+\frac{1-\cos\theta}{\sin\theta}C(k)\right]\right\}\Bigg)\tilde{Q}_c \tag{5a}$$

$$\tilde{f}^C = \rho U^2 b^2[ik\boldsymbol{b}_{cnc} + \boldsymbol{k}_{cnc} + \boldsymbol{k}_{cc}C(k)]\tilde{Q}_c \tag{5b}$$

The acoustic noncirculatory damping and stiffness matrices $\boldsymbol{b}_{cnc}$ and $\boldsymbol{k}_{cnc}$ and the acoustic circulatory stiffness matrix $\boldsymbol{k}_{cc}$ are defined, respectively, as

$$\boldsymbol{b}_{cnc} = \begin{bmatrix} -E_1 \\ E_3 + aE_1 \end{bmatrix}, \quad \boldsymbol{k}_{cnc} = \begin{bmatrix} 0 \\ E_4 - \pi E_5 \end{bmatrix}$$

$$\boldsymbol{k}_{cc} = \begin{bmatrix} -2\pi E_5 \\ 2\pi(\tfrac{1}{2}+a)E_5 \end{bmatrix}$$

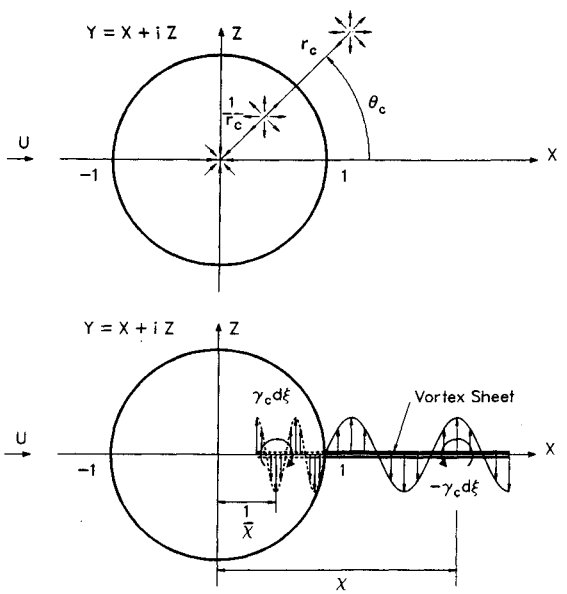

Fig. 2 Schematic showing the noncirculatory and circulatory parts of an acoustically induced flowfield in the Joukowski transformed domain.

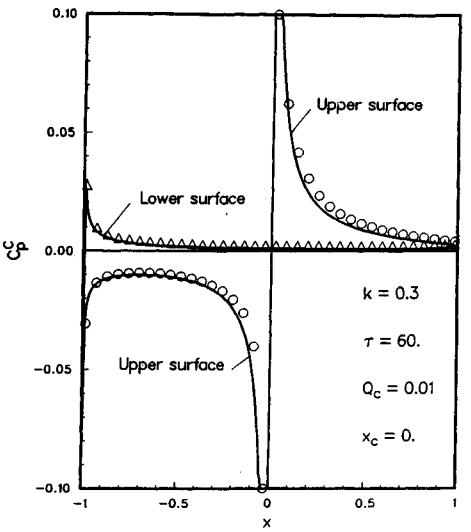

Fig. 3 Comparison of unsteady pressure distributions due to harmonic acoustic excitations: present theoretical solutions, ——; CFD results, o, Δ.

The variables E_1, E_2, E_4, and E_5 appearing in the entries are defined as

$$E_1 = -\frac{\sin\theta_c}{r_c}, \quad E_2 = 0, \quad E_3 = \frac{1}{2}\frac{\sin\theta_c\cos\theta_c}{r_c^2}$$

$$E_4 = -\frac{\sin\theta_c}{r_c}, \quad E_5 = \frac{-1}{\pi}\frac{r_c\sin\theta_c}{1+r_c^2-2r_c\cos\theta_c}$$

At the present time, a computational fluid dynamics approach has been undertaken in parallel with this analytic study in the authors' group. The objective is to build a time-accurate compressible Euler flow solver that can be used to obtain the unsteady loads induced by either a vibrating airfoil or a given acoustic excitation. High-resolution characteristic-based upwind schemes and nonreflective boundary condition treatments were adopted, and a transpired volume flux was used to simulate the sound source located on the surface of the airfoil.[20] Figure 3 illustrates the pressure distributions obtained by the present incompressible analysis and the compressible Euler code ($M_\infty = 0.1$). The agreement is very encouraging, indicating that the derivation is correct. It is worth mentioning that in the inviscid Euler flow code development the Kutta condition is not explicitly enforced.[21] The code produces a smooth flow around the trailing edge because the numerical dissipation plays a similar role as the physical viscosity, leading to the satisfaction of the Kutta condition at the trailing edge.

IV. Trailing-Edge Receptivity

Acoustic sound has been known to be an extremely weak flow perturbation. The use of such a weak fluid power to suppress airfoil flutter has been experimentally demonstrated to be feasible in Ref. 13, and a hydraulic analogy was proposed to explain the underlying physical mechanism. In our opinion, the proposed hydraulic analogy only explained the noncirculatory part that is generated by satisfying the nonpermeable flow condition of a solid body situated in an acoustic field. The circulatory part was not included, which, as will be shown in the subsequent discussions, actually is the dominant part that contributes most to the flutter suppression forces.

Figures 4a and 4b show the real and imaginary parts of the acoustically induced pressure distributions (the subscript denotes partial derivative) that are contributed from both the noncirculatory and the circulatory flowfields. Although the noncirculatory part of the acoustically induced pressure dif-

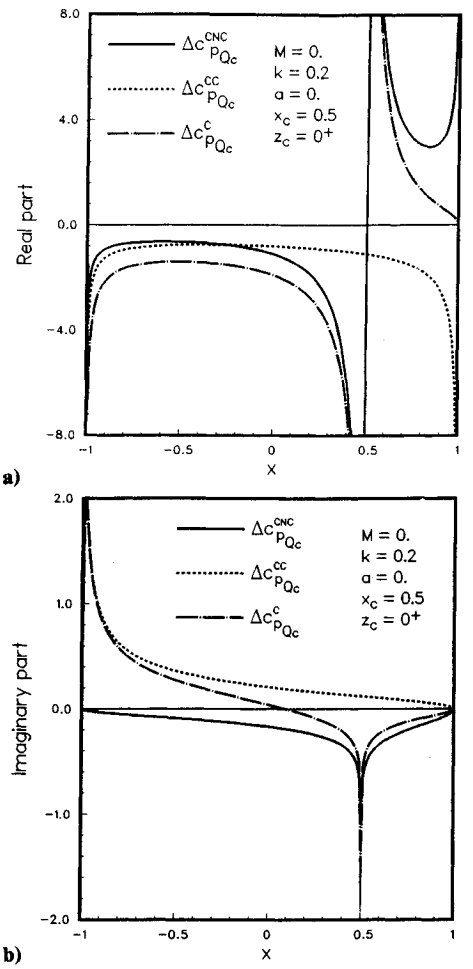

Fig. 4 Acoustically induced noncirculatory, circulatory, and overall pressure differential distributions: a) real parts and b) imaginary parts.

ference, Re (ΔC_p^{CNC}), is comparatively much larger, the fore-and-aft asymmetry makes Re(ΔC_p^{CNC}) contribute actually nothing to the overall lift as it is integrated over the body surface. The resulting lift and pitching moment derivatives are shown in Figs. 5 and 6. It is observed that, if the sound source is not placed in the vicinity of the trailing edge, the noncirculatory pressure distribution contributes significantly only to the real part of the pitching moment. The lift and the important phase-related quantities, Im (C_l) and Im (C_m), however, are all dominated by the circulatory part. Two important messages are delivered in these plots. First, the acoustically induced unsteady lift forces result primarily from the satisfaction of the Kutta condition, i.e., from the circulatory part. In other words, it is the conversion of the incident pressure (acoustic) wave into the vorticity wave shed from the trailing edge that produces the surprisingly large acoustically generated lift forces (bound vortices) around the body. Second, the closer the sound source is located to the trailing edge, the larger the induced airloads will be. This phenomenon, termed *trailing-edge receptivity*, has long been observed and exploited in the mixing, jet, and turbulent flow investigations.[7,8] The sharp edges of the splitter plates, nozzle exits, etc., are known to be the places where disturbances will be amplified together with vorticity waves being generated. The cause for this trailing-edge effect to occur actually lies in the satisfaction of the Kutta smooth flow condition. In flutter problems, the oscillating frequency is usually low enough to apply the Kutta condition. However, modifications of the Kutta condition need to be introduced if the frequency range exceeds certain limits.[14]

The strength of the vortices shed from the trailing edge in response to the incident acoustic waves is a signature representing the effectiveness of the acoustic excitation. Kelvin's theorem states that the unsteady airloads generated around the airfoil are proportional to the strength of the wake shed downstream. A detailed wake flow analysis is presented in the Appendix. The vorticity and downwash distributions in the wake induced by an acoustic monopole on the airfoil surface are shown to take the following forms [compare with Eqs. (A9) and (A10) in the Appendix]:

$$\tilde{\gamma}_w^C(\xi) = \frac{-2}{\pi} \frac{e^{-ik\xi}}{[H_1^{(2)}(k) + iH_0^{(2)}(k)]} \sqrt{\frac{1+x_c}{1-x_c}}\, \tilde{Q}_c$$

[Eq. (A9)]

$$\tilde{w}_w^C(\xi_1) = \frac{1}{2\pi}\sqrt{\frac{\xi_1 - 1}{\xi_1 + 1}} \sqrt{\frac{1+x_c}{1-x_c}} \left\{ \frac{1}{\xi_1 - x_c} + \frac{2}{\pi} \frac{1}{[H_1^{(2)}(k) + iH_0^{(2)}(k)]} F(\xi_1, k) \right\} \tilde{Q}_c$$

[Eq. (A10)]

These shedding vorticity and downwash strengths in the wake are functions of the acoustic excitation location. Examining the functional forms of Eqs. (A9) and (A10), it can be found that $x_c = 1$ (trailing edge) is a singular point and $x_c = 0$ (mid-chord) corresponds to a local extremum. The singular behavior around the trailing edge signifies a rapid increase of the acoustic excitation effectiveness there. This fact supports the concept of trailing-edge receptivity.

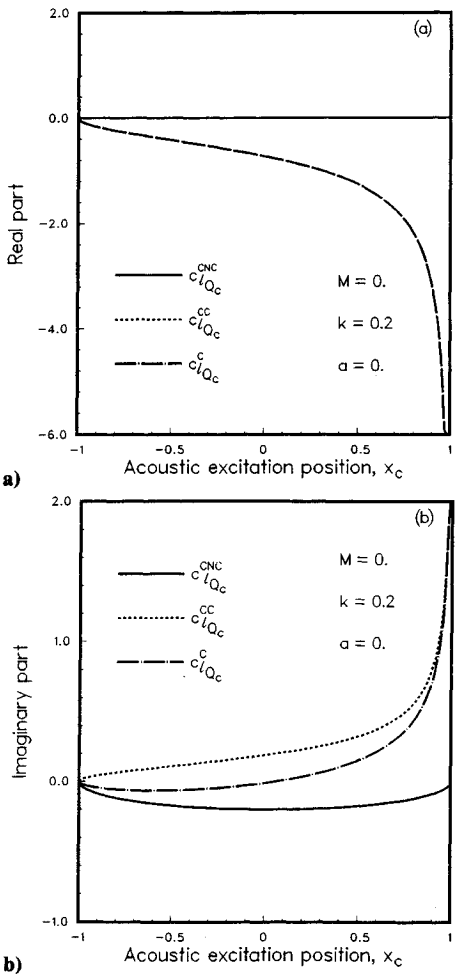

Fig. 5 Acoustically induced noncirculatory, circulatory, and overall lift forces vs acoustic excitation positions: a) real parts and b) imaginary parts.

Based on the previous observations, the sound actually acts as a "catalyst," rather than a direct power, for generating the secondary control field in the flutter suppression process. It is the conversion mechanism around the sharp trailing edge that produces the controlling forces around the solid body that, if driven by a correctly chosen phase relative to the motion of the body, may suppress the fluttering motion.

V. Flutter Suppression Using Active Acoustic Excitations

A. *V-g* Method

In the following, the acoustic excitation frequency is set to be equal to the airfoil flutter frequency to obtain the maximum interferences between the primary and secondary unsteady flowfields. Under the assumption of simple harmonic motions, the governing equations of the oscillating typical section with acoustic excitations located at (x_c, z_c) can be expressed in the frequency domain as

$$\left(\frac{\omega_\alpha}{\omega}\right)^2 \boldsymbol{K}_s \tilde{\boldsymbol{q}} = \left[\boldsymbol{M}_s + \frac{\eta}{k^2}\boldsymbol{A}_a\right]\tilde{\boldsymbol{q}} + \frac{\eta}{k^2}\boldsymbol{A}_c \tilde{\boldsymbol{Q}}_c \tag{6}$$

In Eq. (6), $\boldsymbol{A}_a$ and $\boldsymbol{A}_c$ denote the aerodynamic influence matrices due to the airfoil motions and the acoustic excitation, respectively.

Assuming that the feedback control law takes the form

$$Q_c(t) = \frac{b}{U}\boldsymbol{g}^V \dot{\boldsymbol{q}}(t) + \boldsymbol{g}^D \boldsymbol{q}(t) \tag{7a}$$

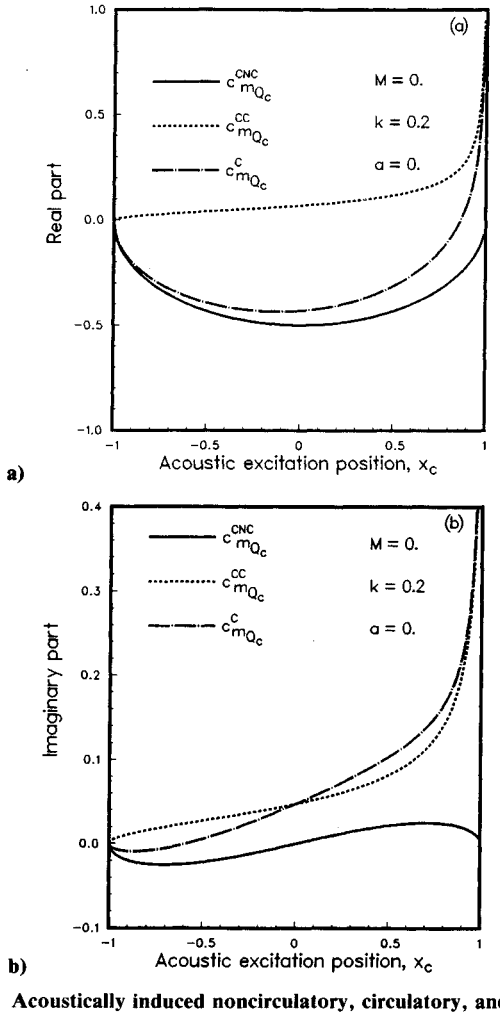

Fig. 6 Acoustically induced noncirculatory, circulatory, and overall pitching moments vs acoustic excitation positions: a) real parts and b) imaginary parts.

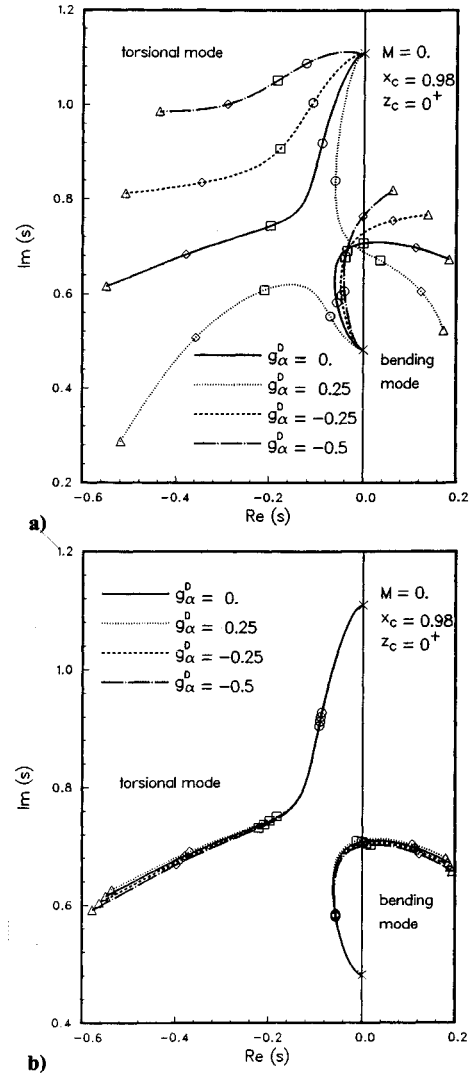

Fig. 7 Roots loci for closed-loop, acoustically controlled flutter suppression tests with control forces a) including both the noncirculatory and circulatory parts, b) including only the noncirculatory part ($\bar{U}$: 0, ×; 2.5, ○; 3.0, □; 3.5, ◇; 4.0, Δ).

where the gain vectors $\boldsymbol{g}^V$ and $\boldsymbol{g}^D$ are defined as

$$\boldsymbol{g}^V = [g_h^V e^{\psi_h^V} \quad g_\alpha^V e^{\psi_\alpha^V}], \qquad \boldsymbol{g}^D = [g_h^D e^{\psi_h^D} \quad g_\alpha^D e^{\psi_\alpha^D}] \tag{7b}$$

In Eqs. (7a) and (7b) we have used the superscripts V and D to denote that the associated variable is either of the "velocity" or of the "displacement" nature. For example, g_h^V and ψ_h^V denote the gain magnitude and phase of the acoustic generator in response to the state of "plunging velocity" $\dot{h}/b$.

The control law, Eq. (7a), can be implemented into Eq. (6), and by introducing an artificial damping constant g, a closed-loop flutter equation may be obtained,

$$(1 + ig)\left(\frac{\omega_a}{\omega}\right)^2 \boldsymbol{K}_s \tilde{\boldsymbol{q}} = \left[\boldsymbol{M}_s + \frac{\eta}{k^2}\boldsymbol{A}_{cl}\right]\tilde{\boldsymbol{q}} \tag{8a}$$

where the closed-loop aerodynamic matrix is given by

$$\begin{aligned}\boldsymbol{A}_{cl} = {} & -k^2(\boldsymbol{M}_{anc} + \boldsymbol{b}_{cnc}\boldsymbol{g}^V) + ik(\boldsymbol{B}_{anc} + \boldsymbol{b}_{cnc}\boldsymbol{g}^D + \boldsymbol{k}_{cnc}\boldsymbol{g}^V) \\ & + (\boldsymbol{K}_{anc} + \boldsymbol{k}_{cnc}\boldsymbol{g}^D) + [ik(\boldsymbol{B}_{ac} + \boldsymbol{k}_{cc}\boldsymbol{g}^V) \\ & + (\boldsymbol{K}_{ac} + \boldsymbol{k}_{cc}\boldsymbol{g}^D)]\, C(k)\end{aligned} \tag{8b}$$

The standard *V-g* method can be employed to solve Eq. (8). The effect of introducing the interfering acoustic field for

flutter suppression can be considered to change the overall aerodynamic matrices, Eq. (8b), and therefore the characteristics of the dynamic system through the appropriately determined feedback control law, Eq. (7).

B. Root-Locus Method

The flutter phenomena governed by the *V-g* method formulation are valid only for the neutral stability condition. As the control of a dynamic system is concerned, it is better to employ the root-locus approach to stretch the region of validity from the imaginary axis to the entire complex domain. Using analytic continuation, by setting $\sigma = ik$ as explained by Sears,[22] the aerodynamic transfer functions obtained based on the assumption of simple harmonic motions can be extended into the entire complex domain, in which the resulting generalized Theodorsen's function $C(\sigma)$, with $\sigma = sb/U$, can be derived accordingly.

The equations of motion of the oscillating typical section with an acoustic excitation can thus be rewritten in the Laplace transform domain as

$$[(\boldsymbol{M}_s - \eta \boldsymbol{M}_{anc})\bar{s}^2 + (-\eta \bar{U}\boldsymbol{B}_{anc})\bar{s} + (\boldsymbol{K}_s - \eta \bar{U}^2 \boldsymbol{K}_{anc}) - (\eta \bar{U}\boldsymbol{B}_{ac}\bar{s} + \eta \bar{U}^2 \boldsymbol{K}_{ac})C(\sigma)]\hat{\boldsymbol{q}} = [\eta \boldsymbol{b}_{cnc}\bar{s} + \eta \bar{U}\boldsymbol{k}_{cnc} + \eta \bar{U}\boldsymbol{k}_{ac}C(\sigma)]\hat{H}_c \tag{9}$$

Similarly, as in the *V-g* method, the control law can be assumed using complex-valued feedback gains:

$$H_c(t) = \frac{1}{\omega_\alpha}\boldsymbol{g}^V \dot{\boldsymbol{q}}(t) + \bar{U}\,\boldsymbol{g}^D \boldsymbol{q}(t) \tag{10}$$

where the gain matrices $\boldsymbol{g}^V$ and $\boldsymbol{g}^D$ are the same ones previously defined in the *V-g* method. With the use of this control law, the equations of motion can be cast into a closed-loop form,

$$[\boldsymbol{A}_2\bar{s}^2 + \boldsymbol{A}_1\bar{s} + \boldsymbol{A}_0 + (\boldsymbol{B}_1\bar{s} + \boldsymbol{B}_0)C(\sigma)]\hat{\boldsymbol{q}} = 0 \tag{11}$$

To render Eq. (11) into a finite-dimensional system that is amenable to stability and control analysis, the generalized Theodorsen's function $C(\sigma)$ must be approximated by some rational functions. The technique developed along the line of Padé approximations has been proved successful.[23-25] The present work adopts the Jones[25] approximation that can be viewed as a Padé approximant using second-order polynomials and is expressed by

$$C(\sigma) = \frac{0.5\sigma^2 + 0.2808\sigma + 0.01365}{\sigma^2 + 0.3455\sigma + 0.01365} \tag{12}$$

Using Eq. (12), the governing equation, Eq. (11), can be rearranged to become

$$(\boldsymbol{P}_4\bar{s}^4 + \boldsymbol{P}_3\bar{s}^3 + \boldsymbol{P}_2\bar{s}^2 + \boldsymbol{P}_1\bar{s}^1 + \boldsymbol{P}_0)\hat{\boldsymbol{q}} = 0 \tag{13}$$

Introducing the state vector $\boldsymbol{x}^T = [\boldsymbol{q}^T, d\boldsymbol{q}^T/d\bar{t}, d^2\boldsymbol{q}^T/d\bar{t}^2, d^3\boldsymbol{q}^T/d\bar{t}^3]$, we now arrive at a first-order dynamic system equation,

$$\frac{d\boldsymbol{x}}{d\bar{t}} = \boldsymbol{A}\boldsymbol{x} \tag{14}$$

It is noticed that the last four states, $d^2\boldsymbol{q}/d\bar{t}^2$ and $d^3\boldsymbol{q}/d\bar{t}^3$, are herein known as the nonphysical augmented states. Only four of the total eight eigenvalues of the system have real physical meanings to be associated with. The flutter boundary and the associated flutter frequency can thus be determined by solving the eigenvalue problem of Eq. (14):

$$(\bar{s}\boldsymbol{I} - \boldsymbol{A})\hat{\boldsymbol{x}} = \boldsymbol{0} \tag{15}$$

Table 1 Summary of flutter results of a typical section model with acoustic excitation ($x_\alpha = 0.2$, $r_\alpha = 0.5$, $\omega_h = 50$ rad/s, $\omega_\alpha = 100$ rad/s, $a = -0.4$, $\mu = 40$, $x_c = 0.98$, $z_c = 0^+$)

		$U_F/b\omega_\alpha$		ω_F/ω_α	
	g_α^D	*V-g* method	Root-locus method	*V-g* method	Root-locus method
Open-loop	0.0	3.0298	3.0032	0.7077	0.7073
Closed-loop[a]	0.25	2.9016	2.8860	0.6879	0.6887
	−0.25	3.2368	3.1921	0.7317	0.7302
	−0.5	3.5932	3.5162	0.7698	0.7665
Closed-loop[b]	0.25	3.0600	3.0327	0.7116	0.7112
	−0.25	3.0005	2.9746	0.7040	0.7036
	−0.5	2.9723	2.9410	0.7005	0.7000

[a] f^C contains both noncirculatory and circulatory parts.
[b] f^C contains only noncirculatory part.

C. Flutter Suppression Tests

To demonstrate that flutter can be suppressed by the application of acoustic excitations, we specifically choose a typical section with the parameters listed in Table 1. The calculated open-loop and closed-loop flutter boundaries and frequencies using both *V-g* and root-locus methods are summarized in Table 1. The results show that the root-locus method, in which an approximate Theodorsen's function is employed, gives slightly smaller flutter boundaries for all of the cases as compared with those obtained by the *V-g* method where the exact Theodorsen function is used. Moreover, the out-of-phase control laws ($g_\alpha^D < 0$) lead to an increase of the flutter boundary, whereas the in-phase control law ($g_\alpha^D > 0$) yields the opposite effect. Using a relatively larger out-of-phase control gain, $g_\alpha^D = -0.5$, the flutter boundary is shown to be enlarged almost 20% above the original open-loop value.

To show that the circulatory part is important for the acoustically induced unsteady airloads, we also list in Table 1 the flutter predictions that use only the noncirculatory part of f^C. It is observed that ignoring the circulatory part will result in quite different flutter boundary predictions, in particular for cases using larger gain constants. This demonstration, added to the previous in-phase and out-of-phase gain studies, implies that the phase-related circulatory contributions of the acoustically induced airloads play a vital role in the flutter suppression mechanism.

Figures 7a and 7b depict the root loci with respect to the airstream velocity. The only difference between these two cases is the aerodynamic model used; one is full and the other contains only the noncirculatory part. It is shown in Fig. 7a that, with the out-of-phase feedback gains ($g_\alpha^D < 0$), the flutter boundary is enlarged and the trajectories follow basically the open-loop behavior; however, in the case of in-phase acoustic excitation ($g_\alpha^D > 0$), the trajectory of the eigenvalues becomes rather different, and the flutter mode changes. The importance of the circulatory part is fully explained in Fig. 7b. Contrary to the trajectories predicted using the full aerodynamic model, all of the root loci in Fig. 7b almost coincide with the open-loop trajectory, implying that the acoustic effect is not correctly accounted for when the circulatory part is neglected. In other words, the mechanism of acoustic flutter suppression in incompressible or low Mach number flows lies in the acoustically induced vortical flow, not the original acoustic wave itself, that changes the characteristics of the dynamic system and stabilizes the fluttering motion.

VI. Parametric Flutter Control Studies

The important parameters that influence the performance of the closed-loop flutter suppression behavior are the control gain magnitude, the phase angles of the gain factor, and the acoustic excitation positions. Here we only present the results related to the gain phases and the acoustic excitation positions. More detailed parametric studies can be found in Ref. 19. Unless otherwise stated, all of the parameters except for the one being discussed will be defaulted zero. In Figs. 8 and

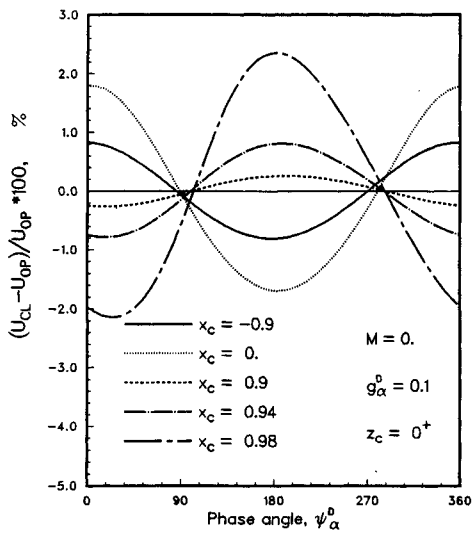

Fig. 8 Effect of feedback gain phase ψ_α^D on flutter boundary variation.

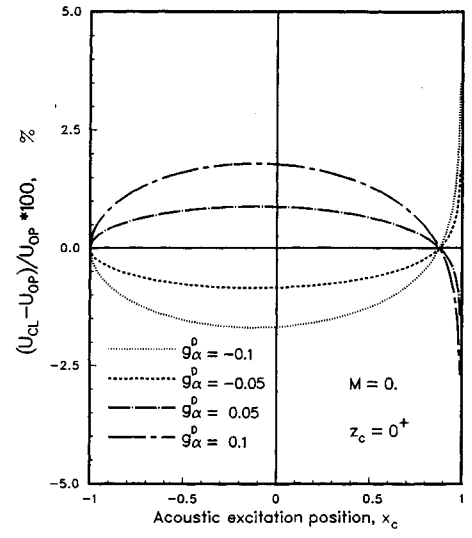

Fig. 9 Effect of acoustic excitation position x_c on flutter boundary variation.

9 the flutter boundary variations will be presented in percentage increment forms, in which the notations U_{op} and U_{cl} represent the open-loop and closed-loop flutter boundaries, respectively.

A. Phase Angles of the Gain Factor

It is commonly acknowledged in the flutter analysis that the phases of the unsteady airloads relative to the vibration of the structure determine whether or not the flutter phenomenon would occur. The success of suppressing a fluttering motion by the use of sound is dependent on the establishment of a destructively interfering secondary field that may modify the primary aerodynamic field and result in an overall dissipative mechanism to the unstable dynamic system. The results, obtained from the *V-g* analyses, are shown in Fig. 8. These optimal phase angles are quite excitation position dependent. For example, in Fig. 8, for a fixed gain phase $\psi_\alpha^D = 0$ deg, the stabilized system with sound source located at $x_c = 0$ could reverse and become even more unstable than the original open-loop system as the excitation position is moved to $x_c = 0.98$.

B. Acoustic Excitation Positions

As demonstrated in the previous unsteady flow analysis, the location of the sound source can critically affect the unsteady aerodynamic flowfield, especially the circulatory part. The flutter boundary improvements in relation to the sound source located on the upper surface of the airfoil, $(x_c, 0^+)$, are calculated and presented in Fig. 9. As expected, the trailing edge is an important region for the acoustic flutter control design. No matter what gain constant is considered, a rapid flutter boundary improvement (or deterioration) occurs as the sound source is placed in the vicinity of the trailing edge. Also indicated in these diagrams is the importance of the phases of the gain constants. A wrong choice of the phase may lead to an unexpectedly low flutter boundary that is highly undesirable and should be avoided.

VII. Concluding Remarks

An analytic derivation of the unsteady, acoustically induced aerodynamic loads for the two-dimensional incompressible flow is developed. It is found that the lift and pitching moment induced by the acoustic excitation are attributed mostly to the circulatory part of the acoustically induced unsteady flowfield. The emitted sound field actually serves as a catalyst rather than a direct control force, that converts the incident pressure wave into the shedding vorticity wave that in turn results in a change of the corresponding circulation around the body. Trailing-edge geometry together with the Kutta condition therefore play a combined critical role in this acoustic control force generation process.

Open-loop flutter analyses and closed-loop flutter suppression control studies are also conducted, using both *V-g* and root-locus methods. A parametric study of the closed-loop dynamics indicates that the phase of the feedback gain constant is a critical factor for determining the stability of the acoustically interfered closed-loop system. Moreover, the enlargement of the flutter boundary can be extraordinary when the locations of the excitations are placed close to the trailing edge. However, this trailing-edge excitation strategy must be used with correct phase angles, otherwise, a dramatic reduction in flutter boundary could occur.

Appendix: Acoustically Induced Vorticity and Downwash Distributions in the Wake

In a harmonically excited two-dimensional incompressible flow, the vorticity distributions along the airfoil and in the wake induced by the downwash $\tilde{w}_a^C(x)$ on the airfoil can be found in standard texts such as Ref. 21 to be

$$\tilde{\gamma}_a^C(x) = \frac{2}{\pi}\sqrt{\frac{1-x}{1+x}}\left\{\int_{-1}^{1}\sqrt{\frac{1+s}{1-s}}\,\frac{\tilde{w}_a^C(s)}{x-s}\,ds\right.$$

$$+\frac{2}{\pi}\,\frac{1}{[H_1^{(2)}(k)+iH_0^{(2)}(k)]}\int_{-1}^{1}\sqrt{\frac{1+s}{1-s}}\,\tilde{w}_a^C(s)\,ds$$

$$\left.\times\int_{1}^{\infty}\sqrt{\frac{\xi+1}{\xi-1}}\,\frac{e^{-ik\xi}}{x-\xi}\,d\xi\right\} \tag{A1}$$

and

$$\tilde{\gamma}_w^C(\xi) = \frac{-4}{\pi}\,\frac{e^{-ik\xi}}{[H_1^{(2)}(k)+iH_0^{(2)}(k)]}$$

$$\times\int_{-1}^{1}\sqrt{\frac{1+s}{1-s}}\,\tilde{w}_a^C(s)\,ds \tag{A2}$$

The downwash in the wake, however, takes the following form:

$$\tilde{w}_w^C(\xi_1) = \frac{1}{\pi}\sqrt{\frac{\xi_1-1}{\xi_1+1}}\left\{\int_{-1}^{1}\sqrt{\frac{1+s}{1-s}}\frac{\tilde{w}_a^C(s)}{\xi_1-s}\,ds + \frac{2}{\pi}\frac{1}{[H_1^{(2)}(k)+iH_0^{(2)}(k)]}\int_1^\infty \frac{e^{-ik\xi}}{\xi_1-\xi}\sqrt{\frac{\xi+1}{\xi-1}} \times \int_{-1}^{1}\sqrt{\frac{1+s}{1-s}}\,\tilde{w}_a^C(s)\,ds\,d\xi\right\} \tag{A3}$$

For a fixed flat plate with a pulsating monopole located at $x = x_c$ on the upper airfoil surface (internal excitation case), the surface boundary conditions are

$$\tilde{w}_a^C(x) = \begin{cases}\tilde{Q}_c\delta(x-x_c) & \text{on } z_c = 0^+\\ 0 & \text{on } z_c = 0^-\end{cases} \tag{A4}$$

Equation (A4) can be further decomposed into symmetric and antisymmetric parts:

$$\tilde{w}_a^C(x,0^\pm) = \tilde{w}_a^I(x,0^\pm) + \tilde{w}_a^{II}(x,0^\pm) \tag{A5}$$

where

$$\begin{aligned}\tilde{w}_a^I(x,0^\pm) &= \tfrac{1}{2}\tilde{Q}_c\delta(x-x_c) \quad \text{(symmetric)}\\ \tilde{w}_a^{II}(x,0^\pm) &= \pm\tfrac{1}{2}\tilde{Q}_c\delta(x-x_c) \quad \text{(antisymmetric)}\end{aligned} \tag{A6}$$

The symmetric part $\tilde{w}_a^I$ will not give rise to any bound and shedding vorticities in contrast to the antisymmetric part $\tilde{w}_a^{II}$. Therefore, the vorticities induced by the acoustic excitation can be viewed as resulting from the downwash on a flat plate:

$$\tilde{w}_a^C(x) = \tfrac{1}{2}\tilde{Q}_c\delta(x-x_c) \tag{A7}$$

Substituting Eq. (A7) into Eqs. (A1) and (A2), we have the acoustically induced vorticity distributions along the airfoil choard and wake, respectively, as

$$\tilde{\gamma}_a^C(x) = \frac{1}{\pi}\sqrt{\frac{1-x}{1+x}}\sqrt{\frac{1+x_c}{1-x_c}}\left\{1+\frac{2}{\pi}\frac{1}{[H_1^{(2)}(k)+iH_0^{(2)}(k)]} \times \int_1^\infty\sqrt{\frac{\xi+1}{\xi-1}}\frac{e^{-ik\xi}}{x-\xi}\,d\xi\right\}\tilde{Q}_c \tag{A8}$$

$$\tilde{\gamma}_w^C(\xi) = \frac{-2}{\pi}\frac{e^{-ik\xi}}{[H_1^{(2)}(k)+iH_0^{(2)}(k)]}\sqrt{\frac{1+x_c}{1-x_c}}\,\tilde{Q}_c \tag{A9}$$

Similarly, substituting Eq. (A7) into Eq. (A3) yields the induced downwash in the wake:

$$\tilde{w}_w^C(\xi_1) = \frac{1}{2\pi}\sqrt{\frac{\xi_1-1}{\xi_1+1}}\sqrt{\frac{1+x_c}{1-x_c}}\left\{\frac{1}{\xi_1-x_c} + \frac{2}{\pi}\frac{1}{[H_1^{(2)}(k)+iH_0^{(2)}(k)]}F(\xi_1,k)\right\}\tilde{Q}_c \tag{A10}$$

where the function $F(\xi_1, k)$ is defined by

$$\begin{aligned}F(\xi_1,k) &= \int_1^\infty\sqrt{\frac{\xi+1}{\xi-1}}\frac{e^{-ik\xi}}{\xi_1-\xi}\,d\xi\\ &= -\int_1^\infty\frac{1}{\sqrt{\xi^2-1}}e^{-ik\xi}\,d\xi + (1+\xi_1)\\ &\quad\times\int_1^\infty\frac{1}{(\xi_1-\xi)\sqrt{\xi^2-1}}e^{-ik\xi}\,d\xi\\ &= \frac{i\pi}{2}H_0^{(2)}(k) + (1+\xi_1)I(\xi_1,k)\end{aligned}$$

and the integral I is defined by

$$\begin{aligned}I(\xi_1,k) &= \int_1^\infty\frac{1}{(\xi_1-\xi)\sqrt{\xi^2-1}}e^{-ik\xi}\,d\xi\\ &= e^{-ik\xi_1}\left[\frac{1}{\sqrt{\xi_1^2-1}}\ln(\xi_1+\sqrt{\xi_1^2-1}) + \frac{\pi}{2}\int_0^k H_0^{(2)}(\zeta)e^{i\xi_1\zeta}\,d\zeta\right]\end{aligned}$$

Acknowledgments

This work was partially suported by the National Science Council under Contract NSC 79-0401-E006-44. The authors gratefully acknowledge the valuable sugestions given by M. F. Platzer, Naval Postgraduate School, and J. M. Wu, University of Tennessee Space Institute, and the reviewers of this journal.

References

[1]Noll, T. E., "Aeroservoelasticity," *Proceedings of the AIAA/ASME/ASCE/AHS/ASC 31st Structures, Structural Dynamics, and Materials Conference* (Long Beach, CA), AIAA, Washington, DC, April 1990, pp. 1560–1570.

[2]Edwards, J. W., Breakwell, J. V., and Bryson, A. E., Jr., "Active Flutter Control Using Generalized Unsteady Aerodynamic Theory," *Journal of Guidance and Control*, Vol. 1, No. 1, 1978, pp. 32–40.

[3]Karpel, M., "Design for Active Flutter Suppression and Gust Alleviation Using State-Space Aeroelastic Modeling," *Journal of Aircraft*, Vol. 19, No. 3, 1982, pp. 221–227.

[4]Nissim, E., "Active Flutter Suppression Using Trailing-Edge and Tab Control Surfaces," *AIAA Journal*, Vol. 14, No. 6, 1976, pp. 757–762.

[5]Ffowcs Williams, J. E., "Anti-Sound," *Proceedings of the Royal Society of London, Series A*, Vol. 395, No. 1808, Sept. 1984, pp. 63–88.

[6]Chu, B.-T., and Kovásznay, L. S. G., "Nonlinear Interactions in a Viscous Heat Conducting Compressible Gas," *Journal of Fluid Mechanics*, Vol. 3, No. 2, 1958, pp. 494–514.

[7]Ho, C.-M., and Huerre, P., "Perturbed Free Shear Layers," *Annual Review of Fluid Mechanics*, Vol. 16, 1984, pp. 365–424.

[8]Culick, F. E. C., "Some Recent Results for Nonlinear Acoustics in Combustion Chambers," AIAA Paper 90-3927, Oct. 1990.

[9]Hsiao, F.-B., Liu, C.-F., and Shyu, J.-Y., "Control of Wall-Separated Flow by Internal Acoustic Excitation," *AIAA Journal*, Vol. 28, No. 8, 1990, pp. 1440–1446.

[10]Epstein, A. H., Ffowcs Williams, J. E., and Greitzer, E. M., "Active Suppression of Compressor Instabilities," AIAA Paper 86-1914, July 1986.

[11]Moore, F. K., "Theory of Multistage Compressors, Parts 1, 2, and 3," *Transactions of ASME, Journal of Engineering for Power*, Vol. 106, No. 4, 1984, pp. 313–336.

[12]Powell, A., "The Noise of Choked Jets," *Journal of the Acoustic Society of America*, Vol. 25, No. 3, 1953, pp. 385–389.

[13]Huang, X. Y., "Active Control of Aerofoil Flutter," *AIAA Journal*, Vol. 25, No. 8, 1987, pp. 1126–1132.

[14]Crighton, D. G., "The Kutta Condition in Unsteady Flow," *Annual Review of Fluid Mechanics*, Vol. 17, 1985, pp. 411–445.

[15]Daniels, P. G., "On the Unsteady Kutta Condition," *Quarterly Journal of Mechanics and Applied Mathematics*, Vol. 31, No. 2, 1978, pp. 49–75.

[16]Bechert, D. W., and Pfizenmaier, E., "Optical Compensation

Measurements on the Unsteady Exit Condition at a Nozzle Discharge Edge," *Journal of Fluid Mechanics*, Vol. 71, No. 9, 1975, pp. 123–144.

[17]Theodorsen, T., "General Theory of Aerodynamic Instability and the Mechanism of Flutter," NACA Rept. 496, 1935.

[18]Bisplinghoff, R. L., Ashley, H., and Halfman, R. L., *Aeroelasticity*, Addison-Wesley, Reading, MA, 1955, Chap. 5.

[19]Huang, L. J., "Optimal Flutter Control of Airfoils Using Active Acoustic Excitation," Ph.D. Dissertation, Inst. of Aeronautics and Astronautics, National Cheng Kung Univ., Tainan, Taiwan, ROC, Dec. 1991.

[20]Lu, P. J., and Yeh, D. Y., "Transonic Flutter Suppression Using Active Acoustic Excitations" (in preparation).

[21]Rizzi, A., "Damped Euler Equation Method to Compute Transonic Flow Around Wing-Body Combinations," *AIAA Journal*, Vol. 20, No. 10, 1982, pp. 1321–1328.

[22]Sears, W. R., "Operational Methods in the Theory of Airfoils in Nonuniform Motion," *Journal of the Franklin Institute*, Vol. 230, No. 7, 1940, pp. 95–111.

[23]Edwards, J. W., "Unsteady Aerodynamic Modeling for Arbitrary Motions," *AIAA Journal*, Vol. 15, No. 4, 1977, pp. 593–595.

[24]Vepa, R., "On the Padé Approximants to Represent Unsteady Aerodynamic Loads for Arbitrary Small Motions of Wings," AIAA Paper 76-17, Jan. 1976.

[25]Jones, R. T., "The Unsteady Lift of a Wing of Finite Aspect Ratio," NACA Rept. 681, June 1941.